Title: Noncontact Ultrasound Elastomocroscopy: Potentials for Assessment for Articular Cartilage

Authors: Yongping Zheng, Minhua Lu, Qing Wang

Address: Department of Health Technology and Informatics, The Hong Kong Polytechnic University

Abstract: Research in elasticity imaging typically relies on 1 to 10 MHz ultrasound. Elasticity imaging at these frequencies can provide strain maps with a resolution in the order of millimeters, but this is not sufficient for applications to skin, articular cartilage, or other fine structures. In this paper, we introduced two methods of noncontact ultrasound elastomicroscopy for imaging the elasticity of biological soft tissues with high resolutions. In the first system, the specimens were compressed using water jet compression. A water jet was used to couple a focused 20 MHz ultrasound beam into the specimen and meanwhile served as a "soft" indenter. Because there was no additional attenuation when propagating from the ultrasound transducer to the specimen, the ultrasound signal with high signal-to-noise ratio could be collected from the specimens simultaneously with compressing process. The compression was achieved by adjusting the water flow. The pressure measured inside the water pipe and that on the specimen surface was calibrated. This system was easily to apply C-scan over sample surfaces. Experiments on the phantoms showed that this water jet indentation method was reliable to map the tissue stiffness distribution. Results of 1D and 2D scanning on phantoms with different stiffness are reported. In the second system, we used osmotic pressure caused by the ion concentration change in the bathing solutions for the articular cartilage to deform them. When bovine articular cartilage specimens were immerged in solutions with different salt concentration, a 50 MHz focused ultrasound beam was used to monitor the dynamic swelling or shrinkage process. Results showed that the system could reliably map the strain distribution induced by the osmotic loading. We extract intrinsic layered material parameters of the articular cartilage using a triphasic model. In addition to biological tissues, these systems have potential applications for the assessment of bioengineered tissues, biomaterials with fine structures, or some engineering materials. Further studies are necessary to fully realize the potentials of these two new methods.

Keywords: ultrasound, biomicroscopy, elasticity imaging, elastomicroscopy, water jet, indentation, ultrasound indentation, osmotic pressure, triphasic model, articular cartilage.

Corresponding author:
Yongping Zheng
Department of Health Technology and Informatics,
The Hong Kong Polytechnic University,
Hung Hom, Kowloon, Hong Kong SAR, P. R. China.
Tel: 852-27667664
Fax: 852-23624365
Email: ypzheng@ieee.org

INTRODUCTION

Tissue elasticity is generally known to be associated with pathologic changes, such as sclerous cancer, edema, degeneration, fibrosis and pressure sore [1-2]. Current research in ultrasonic elasticity imaging of soft tissues typically relies on 1 to 10 MHz ultrasound which is the frequency range used for most medical imaging applications [3]. The spatial resolution obtained at these frequencies (on the order of millimeters) is not sufficient for the study of very fine structures in tissues such as skin layers or articular cartilage [4-7].

Nanoindentation [8] has recently been used for the microscopic mechanical assessment of biological tissues including bone [9], spinal fusion [10], and articular cartilage [11-12]. However, nanoindentation can not provide mechanical properties of tissues at different depths. The testing results are highly dependent on the surface condition of the specimen [10]. Elasticity imaging based on optical coherence tomography (OCT) has also been reported [13-14]. Optical beams are used to probe tissues at different depths, thus images of the scattering intensity from sub-surface structures of soft tissues are obtained to construct strain images [15-16].

High-frequency (20 to 100 MHz) B-mode imaging (ultrasound biomicroscopy) has been widely used in recent years for the assessment of eye tissues, skin, blood vessel, and articular cartilage with an axial resolution of approximately 100 to 20 μm [4]. Elastography of artery walls has been reported using intravascular ultrasound backscattered signals (~30 MHz) obtained while cyclic blood pressure applied a temporally varying loading source on the vessel [17-18]. In other tissues, requiring an external compression source, attempts have been made to acquire high frequency (50 MHz) ultrasound signals while squeezing tissue through a slit in a compressor [6].

However, the slit introduces uncertainties in the mechanical boundary conditions on the specimen and it's difficult to estimate the stress distribution. Fortin et al. [5] used two parallel plates to compress the two sides of cartilage specimens and to collect 50 MHz ultrasound from the open side. Using this configuration, the lateral tissue displacements in one direction were mapped under an axial compression. Based on the ultrasound indentation technique [19-22] using a probe with an in-series ultrasound transducer (frequency ranged from 5 to 15 MHz) and a load sensor, Zheng and coworkers have developed a number of systems for, mapping one-dimensional mechanical properties of articular cartilage (AC) using high frequency ultrasound (20 to 50 MHz) [23-25]. The 2D high-frequency ultrasound elasticity imaging has only been described in theory or using computer simulation in the literature [26-27] because how to properly loading on the tissue samples remains as a problem. In this paper, we introduce ultrasound elastomicroscopy systems, which utilize noncontact loading techniques, one was a mechanical loading using a water jet indentation device and the other was an osmotic loading induced by changing the ion concentration of the bathing solution for the tissue. In both systems, water served as a coupling medium, so that high-frequency focused ultrasound beam could be used to monitor the tissue deformation at a microscopic level. Using our ultrasound elastomicroscopy systems, the strain images at both ultrasound propagation direction and orthogonal direction could be obtained. Furthermore, with the estimated stress distribution, modulus images could also be derived. The system architectures were described. Experimental results on both gel phantoms and bovine articular cartilage were provided and discussed.

METHODS

Ultrasound biomicroscopy for water indentation and osmosis loading

A biomicroscopy system with a frequency range of 10 to 80 MHz was developed. It was comprised of a pulser/receiver (Model 5601A, Panametrics, Waltham, MA, USA), 3D translating device (Parker Hannifin Corporation, Irvine, CA, USA), 500 MHz A/D converter (Model CompuScope 8500PCI, Gage, Canada), PC and custom-developed software. For the water jet indentation system, a bubbler was used to eject a water jet by controlling the water flow (Figure 1). The diameter of the water ejecting nozzle was 1.94 mm. A 20 MHz focused ultrasound transducer with a focal length of 12.7 mm (GE Panametrics, Inc., OH, USA) was fixed with the water ejector and the focused ultrasound beam could propagate through the bubbler when it was full of water as the coupling medium. The transducer and the bubbler were installed to a 3-D translating device which was used to adjust the distance from the nozzle to the specimen surface and to perform 2-D scanning over the tissue. During experiment, specimens were placed on a rigid platform within a water container. A pressure sensor (EPB-C12, Entran Devices, Inc., Fairfield, NJ, USA) was used to measure the water pressure within the water pipe. A load cell (ELFS-T3 mol/L, Entran Devices, Inc., Fairfield, NJ, USA) located under the platform could monitor the overall force applied on the specimen. Both of them were calibrated. The program was used to control the 3D translating device and collect, process and display the ultrasound signal, together with the force and the pressure, in real time during the indentation process. The movement of the transducer and the acquisition of the A-mode ultrasound, force or pressure data were synchronized by the program. The deformation of the specimen under water jet indentation was estimated from the

ultrasound echoes using a cross-correlation algorithm [24]. The modulus was calculated from the water pressure and the deformation as well as the thickness.

For the setup of osmotic loading, a 50 MHz focused ultrasound transducer with a focal length of 12.7 mm, and a focal zone diameter of 0.1 mm (Panametrics, Waltham, MA, USA) and a specially designed container [28]. During the experiment, the saline solution was used as the medium of ultrasound waves to penetrate into cartilage tissues. The specimen was fixed at the bottom of the container and immerged in the saline solution. Using the 3D translating device, the focal zone was first located in the middle of the cartilage layer and then B-scan was conducted to image the cross-section of articular cartilage.

Phantom experiments

Tissue-mimicking phantoms prepared for the experiments were designed as a simple geometry that consisted of a stiff cylindrical inclusion inside a homogeneous background. The phantoms were 25 mm in diameter and 5 mm in height. The stiff inclusion cylinders were made of silicones and their diameter was 8 mm, while the backgrounds were made of agar-water mixture with agar (Fisher Scientific Co. Fairlawn, NJ, USA) concentration ranging from 10.0 g/L to 30.0 g/L. A total of seven phantoms, whose modulus contrast (defined as the ratio of the modulus of the inclusion to that of the background) ranged from 0.97 dB to 10.02 dB, were prepared for the C-scans.

During the water jet scan experiment, the phantom was placed on the platform and slightly fixed to avoid the slip. An area of 12×12 mm^2 was scanned with a step of 0.2 mm, i.e. a total of 3721 indentations were used to image the region of interest. The

pressure during a C-scan was maintained to be a constant. During each scan, the temperature of the water was approximately 20ºC. The scan time for each phantom was at most 20 minutes. Typically, samples were preloaded with a pressure at 3 kPa and were then scanned with a pressure no more than 20 kPa. For each sample, the maximal strain was controlled within 5% and the materials were modeled as linear elastic materials within this strain level. The ultrasound pulsed echoes reflected from the sample surface and bottom were tracked to compose the deformation image. The compressive modulus of each indentation site was estimated from the local stress and strain data with the assumption that the Poisson's ratio of the inclusion and background material were the same. In our measurement, the modulus contrast calculated from the modulus images were compared to the actual values which were measured from the uniaxial compression.

Experiments on articular cartilage

Fresh mature bovine patellae without obvious lesions were obtained within five hours slaughter and stored at –20°C condition until further experiments. The articular cartilage specimen (φ = 6.35 mm) was cored out of the flat area of each cartilage-bone slab using a metal punch. The thickness of the cartilage layer was 1.73 ± 0.42 mm (mean ± SD; n = 14). The specimen was thawed in physiological saline solution (0.15M NaCl) at room temperature (20°C ± 1°C) for three hours to be ready for the experiment. The specimen was fixed at the bottom of the testing chamber on the platform and equi-librated in physiological saline solution for one hour, and then hypertonic saline solution (2 M NaCl) was immediately filled into the container after the 0.15 M saline solution was removed. Sample was equilibrated for another one hour. Then the

solution was quickly changed back to the 0.15 M saline. As the ion concentrations inside and outside the cartilage were different, a Donnan osmotic pressure on the cartilage was generated. The dynamic deformation of the cartilage layer at different depths could be observed in the ultrasound signals. The effects of the osmotic loading to the cartilage specimens were monitored using the ultrasound biomicroscopy system in 1D and 2D.

In this study, the articular cartilage was modeled as a two-layer cylindrical triphasic matrix based on the triphasic theory [29]. All swelling effects were assumed to arise from the electrostatic interaction between negatively charged PGs and ions [30]. According to the depth-dependent strains of the cartilage obtained using the ultrasound measurement and the depth-dependent contents of water and proteoglycan, the mechanical and material parameters were predicted.

RESULTS

Figure 2 shows typical strain and modulus images of a phantom obtained under 4% indentation level (the background's strain level). Figure 3 shows six strain images and corresponding modulus images obtained from the six different phantoms with varying inclusion/background modulus contrast. The modulus contrast was measured by estimating the average modulus inside the inclusion and that inside the background. As the scan area was typically 12 × 12 mm^2 and the inclusion size was 8 mm, the average modulus of the inclusion was obtained from a ROI of 3 × 3 mm^2 at the center of the inclusion and the average modulus of the background was obtained from the average modulus in four ROIs (2 × 2 mm^2) at the four corners of the modulus image. The measured modulus contrast values were compared to those obtained from uniaxial

compression test. It was found that there was a good agreement between the modulus contrast measured from the modulus images and the actual modulus contrast with a correlation coefficient ratio $r = 0.98$.

Figure 4 shows a type M-mode display of the 1D ultrasound monitoring of the cartilage shrinkage induced by the change of the saline from 0.15 M to 2 M. It is obvious that the cartilage surface moved towards the bone. Since the sound speed in cartilage increased as salt gradually moved into the cartilage, the echo from the cartilage-bone interface moved towards the transducer direction. We compensated the change of the sound speed in the strain calculation assuming that the change of the sound speed was uniform throughout the depth direction. The equilibrium swelling strains induced along the depth direction were extracted from the RF ultrasound signals. We observed that the equilibrium swelling strains were not uniform in the depth direction. The largest strain was observed in the middle zone. It is found that the region near the bone has a relatively higher modulus (24.5 ± 11.1 MPa) than the middle zone and the surface layer (7.0 ± 7.4 MPa and 3.0 ± 3.2 MPa, respectively).

Figure 5 shows the result of a type 2D scanning during the shrinkage process of the cartilage induced by the change of saline from 0.15 M to 2 M. To analyze the distribution of the movement of the interstitial tissue at different depth, a region of interest is outlined by the dashed rectangle in the B-mode image shown in Figure 6a. The tissue displacement images during the different periods are formed using the automatic segmentation and 2D tracking method [25]. Figures 6b-d show the changes in the distribution of the displacement of the tissue at different moments. They indicate that the movement of the tissue is large during the beginning phase of the swelling and shrinkage

processes. As time going, the movements of tissues inside cartilage tend to be zero and approach equilibrium.

DISCUSSION AND CONCLUSION

It is still difficult to directly image the strain and modulus distribution of soft tissues at a microscopic level noninvasively. In this paper, we reported two new methods based on ultrasound elastomicroscopy, which can provide strain images at both ultrasound propagation direction and its orthogonal direction in a microscopy level. For the 20 MHz ultrasound used in the water jet indentation, two cycles of damping period, and an ultrasound speed of 1480 m/s [32], the theoretical axial and lateral resolutions were approximately 58 μm and 0.44 mm, respectively [4]. For the 50 MHz ultrasound used in the osmotic loading, the theoretical axial and lateral resolutions were approximately 35 μm and 90 μm, respectively.

The ultrasound water jet indentation system has shown its ability to image the strain and modulus distribution by conducting C-scanning sequences with different pressures. As demonstrated in this study, the modulus images obtained using the water indentation system could be used to effectively identify the stiff inclusions in the phantoms. The modulus contrast measured from the modulus image agreed very well with those obtained using uniaxial compression tests. The contrast resolution of the measurement using this ultrasound water indentation system is related to its ability to differentiate samples having different values of modulus E. If the modulus contrast was defined as the smallest difference of the modulus E between the two samples that was statistically significant, the contrast could be obtained from a statistical analysis using a 95% as 4σ confidence

interval by assuming a normal distribution of the measured modulus E values. For a σ value of 1.68 kPa computed from 35 independent measurement, the contrast resolution was expected to be 6.7 kPa at a 0.05 level of significance. This contrast resolution may satisfy the modulus imaging of most soft tissues [33]. The spatial resolution of the measurements depended on the cross-sectional size and shape of the indenter, as well as the connectivity between the stiff and soft region. In this study, a simple geometry of the phantoms was designed by containing a uniform cylindrical stiff inclusion and a sharp transition of the modulus was assumed at the inclusion/background interface. The distance over which the transition occurred from 10% to 90% of the modulus values between a stiff and a soft region was estimated as the spatial resolution of the system. For the new ultrasound water indentation system with a water jet indenter of 1.94 mm in diameter, the spatial resolution estimated from the modulus profiles was approximately 0.4 mm.

In this study, we have also demonstrated the potentials of using high frequency ultrasound to monitor the swelling or shrinkage of articular cartilage induced by the change of saline concentration in 1D and 2D. We have successfully used dynamic 2D images of cartilage to extract the image of displacement distribution of the tissues. Since no external compression is required to deform the cartilage, this method should have potential for the cartilage assessment, particularly for small specimens. An improved triphasic model was used to describe the 1D depth-dependent equilibrium swelling strain and to extract the aggregated modulus of cartilage. Our results for bovine articular cartilage showed that the swelling-induced strain was a function of the depth. This was similar to the results of the canine and human cadaver cartilage [34, 35].

In spite of the potentials of the two new methods demonstrated by the preliminary results of phantoms and cartilage specimens, a number of issues need to be further investigated before these potentials can be fully realized. We only reported the imaging of overall full-thickness elasticity of the phantoms, though it is possible to map the elasticity distribution in the thickness direction using the ultrasound signals scattered or reflected at different depths. Further investigations are necessary to use real tissues or phantoms embedded with scatterers to demonstrate this potential. On the other hand, the deformation of articular cartilage induced by osmosis loading has been mapped along a cross-section, but we have not demonstrated the ability to map the elasticity of the tissue in a C-scan. Furthermore, we have used triphasic model to obtain layered moduli of cartilage using the osmotic loading, but we could not map the modulus. Studies are being continued to fully realize the potentials of the two techniques. Other issues such as the effect of depth-dependent ultrasound speed in articular cartilage, the theoretical analysis of the interaction between the water jet and the tissue, and the improvement of the signal-to-noise ratio of images are also being investigated. Since both methods use water (it can be saline) as the medium to couple ultrasound beam and to provide the disturbances to the tissue, it is potential to combine these two techniques to provide a more comprehensive assessment for tissues such as articular cartilage. During the swelling or shrinkage of tissues induced by osmosis loading, water jet indentation can be used to continuously monitor the stiffness change.

In summary, we combined high-frequency ultrasound with water jet indentation and osmotic loading to image the mechanical properties of tissues. The

results of phantoms and articular cartilage specimens demonstrated the potentials of the two approaches for mapping the elasticity of tissues in a high resolution. Further studies are required to fully demonstrate their potentials for the tissue assessment.

ACKNOWLEDGEMENTS

This project was partially supported by the Research Grant Council of Hong Kong (PolyU5199/02E, PolyU 5245/03E) and The Hong Kong Polytechnic University.

REFERENCES

1. Mridha M, Odman S. Noninvasive method for assessment of subcutaneous edema. Med Biol Eng Comput 1986; 24: 393–398
2. Garra BS, Cespedes EI, Ophir J, Spratt SR, Zuurbier RA, Magnant CM, Pennanen MF. Elastography of breast lesions: Initial clinic results. Radiology 1997; 202: 79–86.
3. Ophir J, Cespedes I, Ponnekanti H, Yazdi Y, Li X. Elastography: A quantitative method for imaging the elasticity of biological tissues. Ultrasonic Imaging 1991; 13: 111–134.
4. Foster FS, Pavlin CJ, Harasiewicz KA, Christopher DA, and Turnbull DH. Advances in ultrasound biomicroscopy. Ultrasound in Medicine and Biology 2000; 26: 1-27.
5. Fortin M, Buschmann MD, Bertrand MJ, Foster FS, Ophir J. Dynamic measurement of internal solid displacement in articular cartilage using ultrasound backscatter. Journal of Biomechanics 2003; 36: 443-447.
6. Cohn NA, Emelianov SY, Lubinski MA, and O'Donnell M. An elasticity microscope. Part I: Methods. IEEE Transactions on Ultrasonics, Ferroelectrics, and Frequency Control 1997; 44: 1304-1319.
7. Allan E, Pye DA, Levine EL, and Moore JV. Non-invasive pulsed ultrasound quantification of the resolution of basal cell carcinomas after photodynamic therapy. Lasers in medical science.2002; 17: 230-237.

8. Pethica JB, Hutchings R, and Oliver WC. Hardness measurement at penetration depths as small as 20-nm. Philosophical Magazine A - Physics of Condensed Matter Structure Defects and Mechanical Properties 1983; 48: 593-606.
9. Hengsberger S, Enstroem J, Peyrin F, and Zysset Ph. How is the indentation modulus of bone tissue related to its macroscopic elastic response? A validation study. Journal of Biomechanics 2003; 36: 1503-1509.
10. Guo LH, Guo X, Leng Y, Cheng JCY, and Zhang XD. Nanoindentation study of interfaces between calcium phosphate and bone in an animal spinal fusion model. Journal of Biomedical Materials Research 2001; 54: 554-559.
11. Ferguson VL, Bushby AJ, and Boyde A. Nanomechanical properties and mineral concentration in articular calcified cartilage and subchondral bone. Journal of Anatomy 2003; 203: 191-202.
12. Hu K, Radhakrishnan P, Patel RV, and Mao JJ. Regional structural and viscoelastic properties of fibrocartilage upon dynamic nanoindentation of the articular condyle. Journal of Structural Biology 2001; 136: 46-52.
13. Huang D, Swanson EA, Lin CP, Schuman JS, Stinson WG, Chang W, Hee MR, Flotte T, Gregory K, Puliafito CA, and Fujimoto JG. Optical coherence tomography. Science 1991; 254: 1178-1181.
14. Schmitt JM. Optical coherence tomography (OCT): A review. IEEE Journal of Selected Topics in Quantum Electronics 1999; 5: 1205-1215.
15. Schmitt JM. OCT elastography: Imaging microscopic deformation and strain of tissue. Optics Express 1998; 3: 199-211.
16. Bao XD, Zheng YP, Zhao J, and Xiao SJ. Estimation of deformation from OCT images based on multiresolution matching. Proceedings of the Conference on Biomedical Engineering BME2002, Hong Kong, pp. 61-64, 2002.
17. deKorte CL, Cespedes EI, vanderSteen AFW, and Lancee CT. Intravascular elasticity imaging using ultrasound: Feasibility studies in phantoms. Ultrasound in Medicine and Biology 1997; 23: 735-746.
18. de Korte CL, and van der Steen AFW. Intravascular ultrasound elastography: an overview. Ultrasonics 2002; 40: 859-865.

19. Zheng YP and Mak AFT. An ultrasound indentation system for biomechanical properties assessment of soft tissues in vivo. IEEE Transactions on Biomedical Engineering 1996; 43: 912-918.
20. Zheng YP, Mak AFT. Extraction of quasilinear viscoelastic parameters for lower limb soft tissues from manual indentation experiment. ASME Transactions, Journal of Biomechanical Engineering 1999; 121: 330-339.
21. Suh JKF, Youn I, and Fu FH. An in situ calibration of an ultrasound transducer: a potential application for an ultrasonic indentation test of articular cartilage. Journal of Biomechnics 2001; 34: 1347-1353.
22. Laasanen MS, Toyras J, Hirvonen J, Saarakkala S, Korhonen RK, Nieminen MT, Kiviranta I, Jurvelin JS. Novel mechano-acoustic technique and instrument for diagnosis of cartilage degeneration. Physiological Measurement 2002; 23: 491-503.
23. Zheng YP, Ding CX, Bai J, and Mak AFT. Measurement of nonhomogeneous compressive properties of trypsin treated articular cartilage: An ultrasound investigation. Medical and Biological Engineering and Computing 2001; 39: 534-541.
24. Zheng YP, Mak AFT, Lau KP, Qin L. An ultrasonic measurement for in vitro depth-dependent equilibrium strains of articular cartilage in compression. Physics in Medicine and Biology 2002; 47: 3165-3180.
25. Zheng YP, Bridal SL, Shi J, Saied A, Lu MH, Jaffre B, Mak AFT, and Laugier P. High Resolution Ultrasound Elastomicroscopy Imaging of Soft Tissues: System Development and Feasibility. Physics in Medicine and Biology 2004; 49: 3925-3938.
26. Konofagou EE, Harrigan TP, Ophir J, Krouskop TA. Poroelastography: Imaging the poroelastic properties of tissues. Ultrasound in Medicine and Biology 2001; 27: 1387-1397.
27. Righetti R, Ophir J, and Ktonas P. Axial resolution in elastography. Ultrasound in Medicine and Biology 2002; 28: 101-113.
28. Zheng YP, Shi J, Qin L, Patil SG, Mow VC, Zhou KY. Dynamic depth-dependent osmotic swelling and solute diffusion in articular cartilage monitored using real-time ultrasound. Ultrasound in Medicine & Biology 2004; 30: 841-849.

29. Lai WM, Hou JS, Mow VC. A triphasic theory for the swelling and deformation behaviors of articular cartilage. Journal of Biomechanical Engineering 1991; 113: 245-258.
30. Niu HJ, Wang Q, Zheng YP. Extraction of modulus from the osmotic swelling of articular cartilage measured using ultrasound. 3rd International Conference on the Ultrasonic Measurement and Imaging of Tissue Elasticity, Cumbria, UK. Oct 17-20 2004. pp.115.
31. Lu MH, Zheng YP, Huang QH. A novel noncontact ultrasound indentation system for measurement of tissue material properties using water jet compression. Ultrasound in Medicine and Biology 2005; 31: 817-826.
32. Krautkramer J and Krautkramer H. Ultrasonic testing of materials. 1969; New York: Springer-Verlag.
33. Krouskop TA, Dougherty DR, Vinson FS. A pulsed Doppler ultrasonic system for making noninvasive measurement of the mechanical properties of soft tissue. J Rehab Res Biol 1987; 14:1–8
34. Narmoneva DA, Wang JY, Setton LA. Nonuniform swelling-induced residual strains in articular cartilage. J Biomech 1999; 32: 401-408.
35. Narmoneva DA, Wang JY, Setton LA. A noncontacting method for material property determination for articular cartilage from osmotic loading. Biophys J 2001; 81: 3066-3076.
36. Maroudas A. Balance between swelling pressure and collagen tension in normal and degenerate cartilage. Nature 1976; 260: 808-809.
37. Mow VC, Zhu W, Ratcliffe A. Structure and function of articular cartilage and meniscus. In: Mow, V.C., Hayes, W.C., (Eds.), Basic Othopaedic Biomechanics. New York: Raven Press, 1991; pp. 143-198.

Figure Captions:

Fig. 1. Diagram of the ultrasound water jet indentation system. The water jet was used as an indenter and focused high-frequency ultrasound was employed to monitor the deformation of the soft tissue. The 3D translating device facilitated the system to easily apply C-scan for the soft tissue. By applied different pressure during C-scan sequences, the modulus image was obtained with the recorded pressure, deformation and thickness.

Fig. 2. Typical (a) strain and (b) modulus images of a phantom with a stiff inclusion (the diameter of the inclusion was 8 mm) obtained under 4% indentation level (background's strain level).

Fig. 3. Strain and corresponding modulus images obtained from the six different phantoms of varying inclusion/background modulus contrast. The measured modulus contrast was 9.61, 8.96, 7.71, 3.95, 1.32, 0.10 dB for the six phantom (CP1 to CP6), respectively.

Fig. 4. A typical A-mode and M-mode display of the ultrasound signal collected from the articular cartilage after the concentration was changed from 0.15 to 2 M. The images were sampled at a rate of approximately 0.8 s per frame.

Fig. 5. (a) A B-mode ultrasound image of the cartilage cross-section. The grey levels of the image linearly represent the amplitude of the RF signals. The images were sampled at a rate of approximately 0.8 s per frame. The image of displacement distribution of the region of interest indicated by the dashed rectangle (divided into 15 × 40 segments) in (a) are calculated using the 2D a cross-correlation tracking method. The displacement distribution of articular cartilage extracted from the 2D images obtained at (a) 2.5 min and 4.2 min, (b) 5.8 min and 7.5 min, and (d) 10.8 min and 12.5 min. The grey levels of images (b-c) represent the displacement value of the segments at two moments during the shrinkage phase.

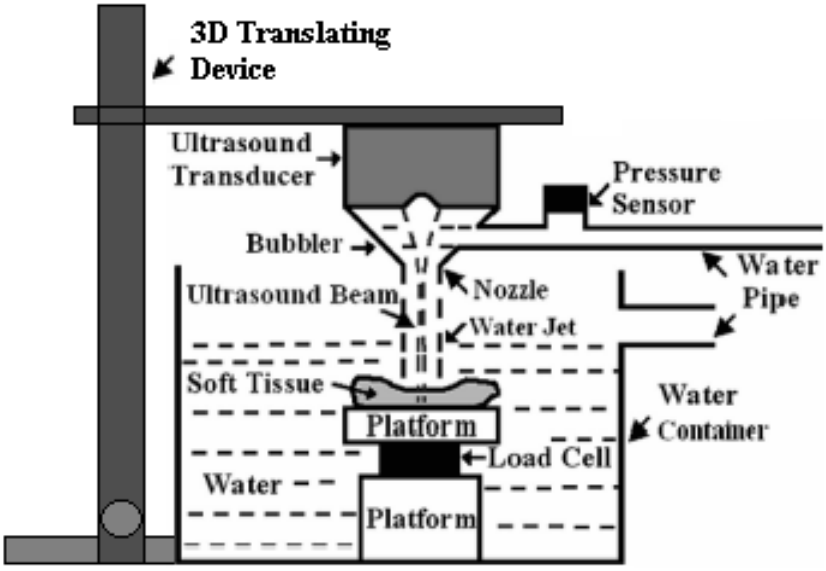

Fig. 1.

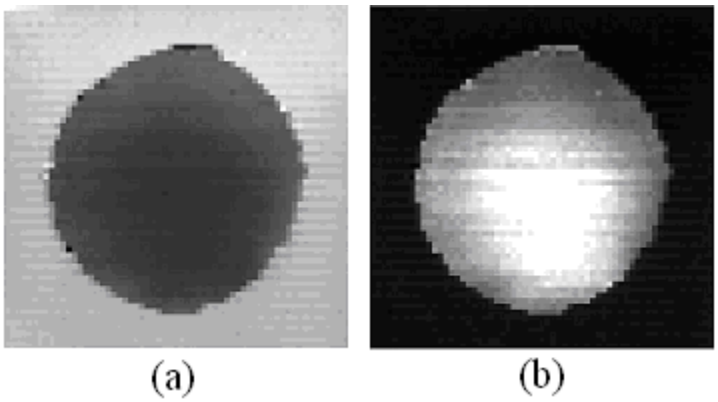

Fig. 2.

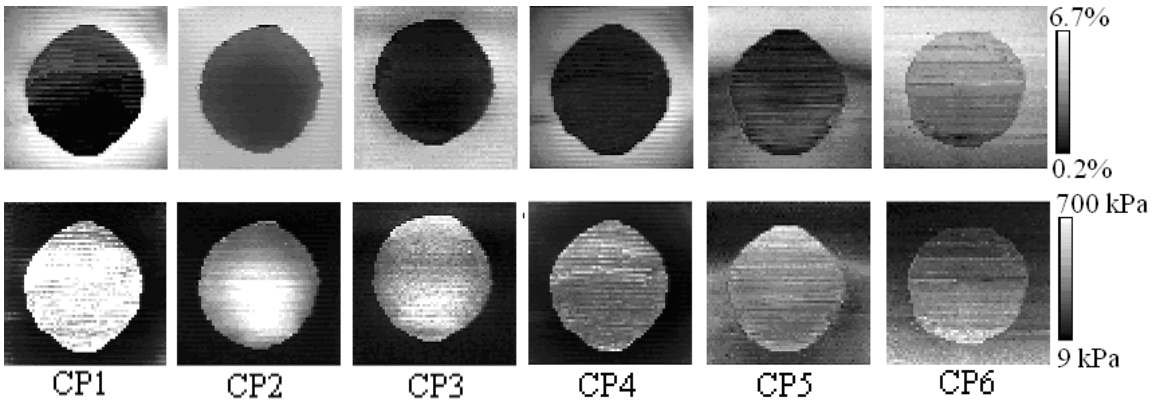

Fig. 3.

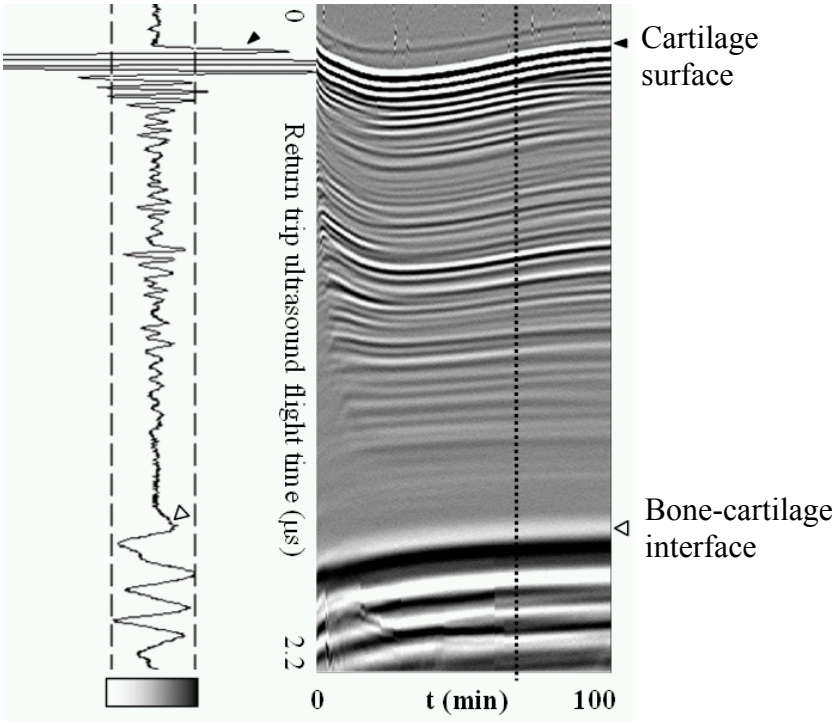
0
Return trip ultrasound flight time (μs)
2.2
0
t (min)
100
Cartilage surface
Bone-cartilage interface

Fig. 4.

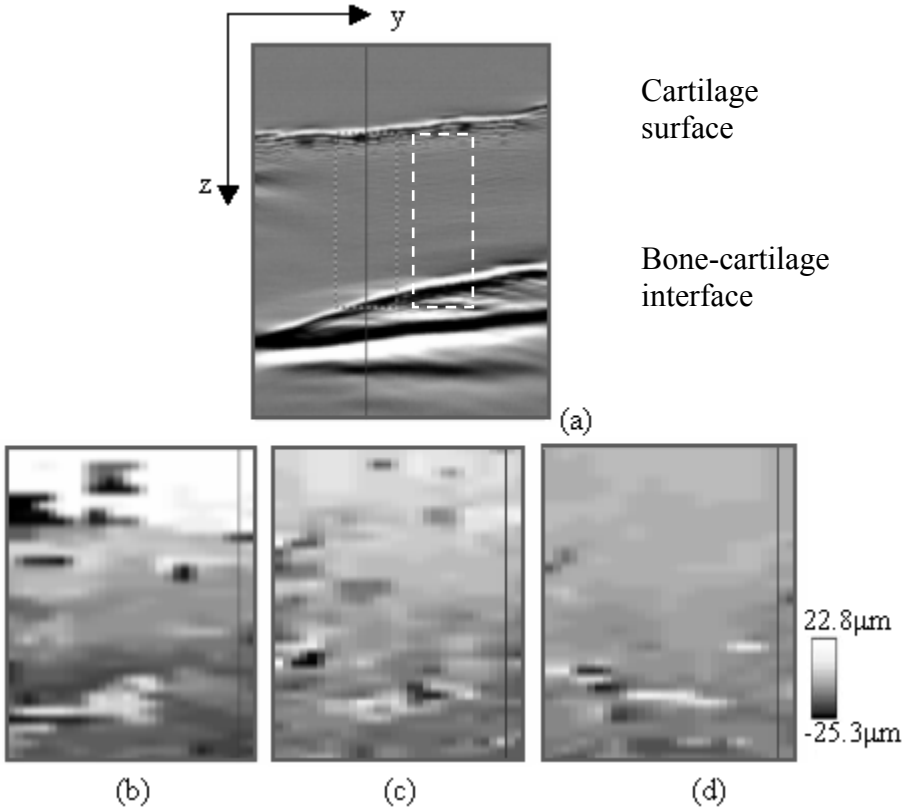
y
z
Cartilage surface
Bone-cartilage interface
(a)
22.8μm
-25.3μm
(b)
(c)
(d)

Fig. 5.